Lawrence Berkeley National Laboratory
Recent Work

Title
Variability in observed stable water isotopes in snowpack across a mountainous watershed in Colorado

Permalink
https://escholarship.org/uc/item/0v03x58p

Journal
Hydrological Processes, 36(8)

ISSN
0885-6087

Authors
Carroll, Rosemary WH
Deems, Jeffery
Maxwell, Reed
et al.

Publication Date
2022-08-01

DOI
10.1002/hyp.14653

Peer reviewed

eScholarship.org Powered by the California Digital Library
University of California

Check for updates

Received: 2 December 2021 | Revised: 8 June 2022 | Accepted: 27 June 2022

DOI: 10.1002/hyp.14653

RESEARCH ARTICLE

WILEY

Variability in observed stable water isotopes in snowpack across a mountainous watershed in Colorado

Rosemary W. H. Carroll[1] | Jeffery Deems[2] | Reed Maxwell[3] | Matthias Sprenger[4] | Wendy Brown[5] | Alexander Newman[5] | Curtis Beutler[5] | Markus Bill[4] | Susan S. Hubbard[4] | Kenneth H. Williams[4]

[1]Desert Research Institute, Reno, Nevada, USA

[2]National Snow and Ice Data Center, Boulder, Colorado, USA

[3]Princeton University, Princeton, New Jersey, USA

[4]Lawrence Berkeley National Laboratory, Berkeley, California, USA

[5]Rocky Mountain Biological Laboratory, Gothic, Colorado, USA

Correspondence
Rosemary W. H. Carroll, Division of Hydrologic Sciences, Desert Research Institute, 2215 Raggio Parkway, Reno, NV 89512, USA.
Email: rosemary.carroll@dri.edu

Funding information
US Department of Energy Office of Science, Grant/Award Number: DE-AC02-05CH11231

Abstract

Isotopic information from 81 snowpits was collected over a 5-year period in a large, Colorado watershed. Data spans gradients in elevation, aspect, vegetation, and seasonal climate. They are combined with overlapping campaigns for water isotopes in precipitation and snowmelt, and a land-surface model for detailed estimates of snowfall and climate at sample locations. Snowfall isotopic inputs, describe the majority of $\delta^{18}O$ snowpack variability. Aspect is a secondary control, with slightly more enriched conditions on east and north facing slopes. This is attributed to preservation of seasonally enriched snowfall and vapour loss in the early winter. Sublimation, expressed by decreases in snowpack d-excess in comparison to snowfall contributions, increases at low elevation and when seasonal temperature and solar radiation are high. At peak snow accumulation, post-depositional fractionation appears to occur in the top 25 ± 14% of the snowpack due to melt-freeze redistribution of lighter isotopes deeper into the snowpack and vapour loss to the atmosphere during intermittent periods of low relative humidity and high windspeed. Relative depth of fractionation increases when winter daytime temperatures are high and winter precipitation is low. Once isothermal, snowpack isotopic homogenization and enrichment was observed with initial snowmelt isotopically depleted in comparison to snowpack and enriching over time. The rate of $\delta^{18}O$ increase (d-excess decrease) in snowmelt was 0.02‰ per day per 100-m elevation loss. Isotopic data suggests elevation dictates snowpack and snowmelt evolution by controlling early snow persistence (or absence), isotopic lapse rates in precipitation and the ratio of energy to snow availability. Hydrologic tracer studies using stable water isotopes in basins of large topographic relief will require adjustment for these elevational controls to properly constrain stream water sourcing from snowmelt.

KEYWORDS
Colorado, d-excess, mountains, snowfall, snowmelt, snowpack, stable water isotopes

1 | INTRODUCTION

Snow-dominated headwaters provide water resources to one-sixth the world's population (Barnett et al., 2005) and support a wide range of ecologic and social-economic services (Immerzeel et al., 2020). Despite their importance, there is only a moderate understanding of how much snowfall makes it to streamflow and how these systems may change with climate and land use alteration. Stable isotopes of

 © 2022 John Wiley & Sons Ltd.

water ($^{18}O/^{16}O$, $^{2}H/^{1}H$) have the potential to provide insight on sourcing and have long been used as natural tracers to assess water partitioning (Berkelhammer et al., 2020; Carroll et al., 2018; Jasechko, 2019; Vreča & Kern, 2020). However, mountainous watersheds likely experience strong spatial and temporal gradients in isotopic composition in snowpack and associated snowmelt and detailed empirical studies to assess this isotopic variability are limited. This is primarily due to the difficulty in measuring isotopic compositions across relatively small spatial–temporal scales important to snow processes in seasonally dynamic and topographically complex basins (Bales et al., 2006; Broxton et al., 2015; Clark et al., 2011; Tennant et al., 2017). An added complication arises given most snow resides near treeline (Carroll et al., 2019; Mott et al., 2018). Regular and safe access for field work in these environments is often not possible and field equipment installations struggle in the harsh climate (Varadharajan et al., 2019). Because of data collection challenges, mass-balance isotope mixing models in snow-dominated, mountainous terrain tend to aggregate limited snow data to define oxygen and hydrogen stable isotope relationships between bulk snowpack to snowmelt (Bearup et al., 2014; Carroll et al., 2018; Evans et al., 2016; Fang et al., 2019). The extrapolation of isotopic inputs from these smaller plot-scale approaches across a larger, mountainous watershed may introduce significant error into mass balance analyses tracking snow water to streamflow.

Extrapolation of stable isotope ratios sampled at study plots to catchment scales is hindered by the uncertainty in isotope ratios during deposition, as well as spatially variable post-depositional processes. A comprehensive review on processes affecting isotopic characteristics in snowpack and associated snowmelt is provided by Beria et al. (2018). In brief, precipitation isotopic inputs are largely controlled by origin of air mass with variation dictated by cloud processes and Rayleigh distillation effects along its trajectory (Bowen et al., 2019; Clark & Fritz, 1997). Stable isotopes in precipitation, particularly at continental locations during the winter, have long been understood to covary with air temperature (Bowen, 2008). Locally, there are sub-seasonal storm variability and strong altitudinal effects; but in general, heavy isotopes are at a maximum in summer and a minimum in winter (Clark & Fritz, 1997). As a result, rain will plot to the right of snow in the dual isotope space (plot of δ^2H vs. $\delta^{18}O$; Figure 2 in Beria et al., 2018). After deposition, the isotopic content in the snowpack can vary due to diffusional transport of water from the soil, temperature-gradient induced vapour diffusion within the snow column, lateral flow through the snowpack, and fractionation processes associated with sublimation and melt-freeze cycles (Beria et al., 2018; Cooper, 1998; Evans et al., 2016; Friedman et al., 1991; Sinclair & Marshall, 2008; Stichler et al., 1981). Once the snowpack is isothermal, the snowpack homogenizes isotopically with accelerated downward progress of melt-freeze cycles in combination with the upward flux of vapour (Friedman et al., 1991; Taylor et al., 2001; Unnikrishna et al., 2002).

Water vapour loss via sublimation is a potentially important component of snowpack water balance (Lang, 1981; MacDonald et al., 2010) with estimates of snow water loss highly variable in mountain systems (Jackson & Prowse, 2009; Svoma, 2016). For high altitude sites located in the continental interior of North America, sublimation estimates range from 15% (Hood et al., 1999) to 28% peak snow accumulation and with relative amounts increasing during low snow years (Sexstone et al., 2018). Sublimation is predominant during the accumulation season (Earman et al., 2006) to preferentially enrich heavier isotopes on the snowpack surface (Stichler et al., 1981). This is due to kinetic processes associated with liquid-to-vapour phase shifts driven by molecular mass differences between ^{18}O and ^{2}H (Clark & Fritz, 1997). The effect of kinetic fractionation is commonly represented by the second-order isotopic parameter d-excess (d-excess $= \delta^2H - 8 * \delta^{18}O$). D-excess expresses the deviation from the global meteoric water line (GMWL) (Dansgaard, 1964) with values less than 10‰ often indicative of kinetic fractionation due to evaporation or sublimation.

During snowpack ablation and periods of high solar radiation, melt fractionation can become the dominant process of snowpack metamorphism (Earman et al., 2006). Isotopic exchange between water and ice at equilibrium (and 0°C) produces a −3.0‰ and −19.5‰ for $\delta^{18}O$ and δ^2H, respectively, in water compared to ice (O'Neil, 1977). Subsequently, snowmelt is more depleted than the bulk snow condition from which it originates. From a mass balance perspective, the removal of depleted snowmelt produces a more enriched snowpack. As melt progresses, the snowpack and corresponding snowmelt become progressively enriched (Taylor et al., 2001).

To investigate first-order controls on observed snowpack and snowmelt isotopic variability, we collected stable water isotopic information from 81 snowpits over a 5-year period across a large mountainous watershed in the Upper Colorado River Basin. Data spans gradients in elevation, aspect, vegetation, and seasonal climate condition and will help constrain future research focused on plant water use strategies and streamflow sourcing. We combine these data with overlapping campaigns for stable water isotopes in precipitation and snowmelt, and a land-surface model to estimate daily climate and isotopic inputs related to snowfall at each sample location. Through statistical analysis of the data, we ask: (1) what are the dominant predictor variables of bulk isotopic content in snowpack near peak accumulation; (2) can we identify post-depositional processes on snowpack isotopic content as a function of landscape position and/or climate condition; and (3) how does snowpack and snowmelt evolve across elevation?

2 | SITE DESCRIPTION

The East River, Colorado is a headwater basin of the Colorado River in the southwestern United States (ER, 750 km^2, Figure 1). Elevations span 2440–4300 m and contain pristine alpine, subalpine, montane, and riparian ecosystems. Climate is defined as continental subarctic with long, cold winters and short, cool summers. Two snow-telemetry (SNOTEL) sites occur within the ER at elevations 3243 m (Schofield) and 3106 m (Butte). Precipitation at Schofield (period of record,

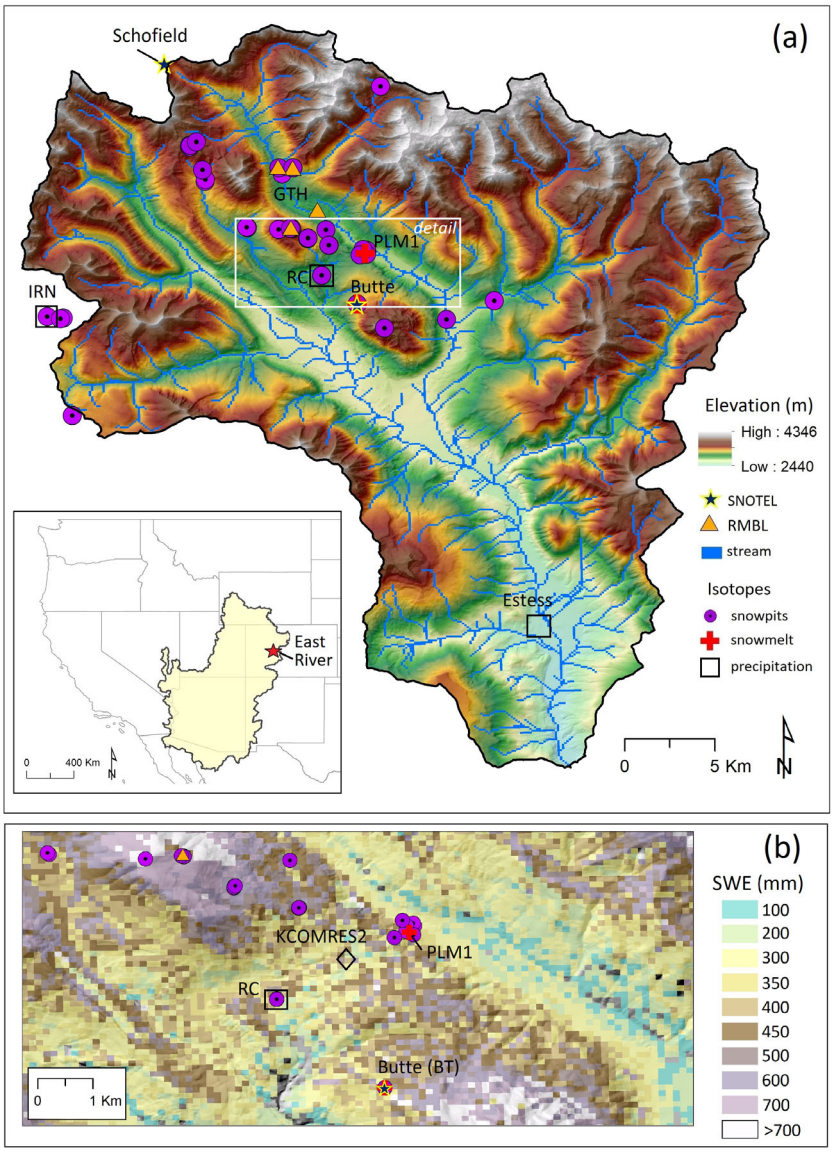

FIGURE 1 (a) The East River Watershed with sampling locations, and (inset) with respect to the Colorado River Basin in the western United States. (b) Detail of the land-surface model 100-m grid with estimated snow water equivalent (SWE) 7 April 2019 (refer to methods and SI for details)

1986–2020) is 1220 ± 245 mm/year, with Butte precipitation half (630 ± 143 mm/year). On average, snowfall accounts for 80% of water inputs to the basin (Carroll et al., 2020). The snow accumulation period is assumed to begin 1 October with peak snow water equivalent (SWE) traditionally defined on 1 April. On average, peak SWE at Schofield is 962 ± 262 mm. Temperatures at Schofield are at a minimum in January (−8.9 ± 4.4°C) and a maximum in July (11.4 ± 2.1°C). Snow seasons considered in this study are 2016–2020. Winter in 2016 represents average snow conditions, while 2018 and 2019 represent dry and wet conditions, respectively. The warmest winters occurred in 2017 and 2018, while 2019 represents the coolest winter.

3 | DATA AND METHODS

We measured stable water isotope ratios in precipitation, snowpack, and snowmelt. All water samples for stable isotope analysis were placed in 1.5 ml glass vials with Teflon™ coated septa lids. Hydrogen and oxygen isotope ratios of water collected 2016–2018 were measured using an Off-Axis Integrated Cavity Output Spectrometer coupled to an autosampler interfaced with a heated injector block (Los Gatos Research, San Jose, USA). Samples collected in 2019 and 2020 were processed with a Picarro L2130-i isotope and gas concentration analyser. Hydrogen and oxygen isotope ratios are reported as the ratio (R) of concentration of heavier to lighter isotopes (e.g., $^{18}O/^{16}O$) and standardized relative to the Vienna Standard Mean Ocean Water (VSMOW). Results are presented in conventional δ-notation in units of per mil (‰),

$$\delta = 1000 * \frac{R_{sample} - R_{VSMOW}}{R_{VSMOW}}. \quad (1)$$

3.1 | Precipitation

Precipitation isotope samples were collected at site RC (Figure 1) from August 2014 to August 2016 and identified as rain ($n = 70$) or snow/

mixed ($n = 60$). Samples were collected using a plastic container rinsed three times with distilled water. The container was installed upon the initiation of a precipitation event and removed once ample water accrued for analysis (1–5 min). The method did not capture storm totals but did remove potential effects of evaporation on the sample. Data were used to construct the local meteoric water line (LMWL). Daily isotopic values in precipitation at the site were then estimated using observed daily meteorologic forcing. The regression analysis was based on linear least squares and evaluated using the Alkaike Information Criteria (AIC), coefficient of determination, and statistical significance. The AIC approach ranks the relative ability of a model to replicate observed behaviour by assessing if added information is sufficient to avoid overfitting. The statistical model considered daily observations of air temperature from the Butte SNOTEL, as well as dew point, relative humidity, and wind speed obtained from KCOMTRE2 (https://www.wunderground.com/dashboard/pws/KCOMTCRE2, Figure 1b). Three snowfall sampling sites were established October 2020 across an elevation gradient (Figure 1, IRN, RC, Estess) and used to develop an isotopic elevational lapse rate for the basin. Collectors were 1 m tall, 15 cm diameter PVC tubes with a capped bottom and 10 cm wire wind/bird baffle at the top. Samples were collected weekly to limit effects of evaporation.

3.2 | Snowpack

Snowpack stable water isotopes observations span elevations 2723–3596 m (Figure 1). During years 2016–2019, 48 snowpits were sampled at peak SWE, and five snowpits were sampled prior to or after peak accumulation. In 2020, two locations were sampled bi-weekly from January to full melt (Figure 1). The IRN site (3191 m) was in the upper subalpine with low-density conifer. The GTH site (2923 m) was in the lower subalpine in an open area containing no vegetation. A third location was added at RC in late March 2020 representing the lower subalpine for ease of access during the onset of COVID-19. These data are provided in the data package but did not provide additional information beyond the GTH site and are not discussed here. All snowpits were dug in flat areas with samples collected in duplicate at 10-cm depth increments to tabulate snow density, temperature, and isotopic content. Bulk snowpack isotopic content is the SWE-weighted composite value across the entire snow column. Snowpits collected over time in 2020 were dug along rows within a 100 m $\times$ 20 m area to alleviate disturbance from previous snowpits but maintain similar snow conditions across samples.

Statistical analysis for observed isotopic content of snowpack near peak SWE was performed across multiple scales. Specifically, we address the following: (i) basin-wide, annually average, bulk snowpit; (ii) bulk value for individual snowpits; (iii) basin-wide, annually averaged values as a function of snowpit depth; (iv) depth profiles for individual snowpits. Observed snowpack isotopic values were compared to winter precipitation inputs estimated with a land-surface model (Section 3.4) and isotopic content in precipitation (Sections 3.1 and 4.1) to assess the potential for post-depositional metamorphism in the snowpack. Precipitation estimates for sampling sites located slightly outside the land-surface model domain used simulated snowfall for the most proximal cell in the land-surface model that matched the elevation, aspect, and vegetation of the actual sample site. Multiple linear regression models are based on ranked correlation statistics with parameters defining geographic position (UTM), topography (USGS, 2019), vegetation characteristics and seasonal climate variables. Regression model efficacy was evaluated using AIC and standard analysis of variance techniques.

3.3 | Snowmelt

Snowmelt was evaluated at two locations in 2017 (Figure 1). The BT snowmelt site (3106 m) was adjacent to the Butte SNOTEL and located in a subalpine conifer forest. The PLM1 snowmelt site (2789 m) was in the lower montane and dominated by shrubs. The sampling system used a modified version of Kormos (2005). Specifically, two five-gallon plastic buckets, each approximately 0.5 m in height, were connected bottom-to-top, with small holes drilled into the bottom of the upper-most bucket to allow melting snow to drain into the lower, or reservoir, bucket. The bucket-system was buried in the ground to the top of the reservoir bucket, with the upper-most container remaining above the ground surface. The system design limits effects of laterally moving snowmelt into the reservoir. Mineral oil was used to avoid possible evaporative effects post snowmelt, and a PVC tube was positioned into the reservoir with the option to extend/shorten length based on the depth of snowpack. Tubing for a peristaltic pump was threaded through the PVC tube to access the reservoir. The simple system was sampled weekly beginning 1 April until full melt was achieved.

3.4 | Land-surface model

The land-surface model was developed to track snowfall, SWE, air temperature and incident solar radiation at each snowpit location. The land-surface model is the semi-empirical, spatially distributed Precipitation-Modelling Runoff System (PRMS, Markstrom et al., 2015). Water and energy are tracked daily through the atmosphere, canopy, surface and subsurface at a 100 m grid resolution. Vegetation cover type, canopy density and winter transmissivity of solar radiation were calculated using techniques presented by Gardner et al. (2018) based on vegetation classification maps (Breckheimer, 2021; Landfire, 2015). The distribution of air temperature used a daily elevational lapse rate of minimum and maximum temperature between the two SNOTEL stations and adjusted for aspect. Shortwave solar radiation used a modified degree-day method developed in the Rocky Mountain region and applicable for sites with clear skies on days that lack precipitation (Leavesley et al., 1983). Solar radiation was calibrated to match observations at four weather stations operated by the Rocky Mountain Biological Laboratory (RMBL, Figure 1). Observed precipitation at the Schofield SNOTEL was spatially

TABLE 1 Regression models for daily precipitation at the RC site and bulk snowpack across the East River for $\delta^{18}O$ and d-excess

Type	Isotope	Phase	Equation	Parameter	Description	Units	*p*-value	ρ
Daily precipitation	$\delta^{18}O$	Snow	$0.60T - 17.34$	T	Air temperature[a]	°C	0.000	0.57
		Rain	$1.09T + 0.62W - 17.34$	T	Air temperature[a]	°C	0.000	0.56
				W	Wind speed[a]	kph	0.008	0.13
	d-excess	Snow	$0.26T + 14.55$	T	Air temperature[a]	°C	0.052	0.25
		Rain	$-0.74T + 0.27Rh - 5.06$	T	Air temperature[a]	°C	0.000	−0.33
				Rh	Relative humidity[a]	%	0.008	0.43
Bulk snowpit	$\delta^{18}O$	Snow	$0.15TxN + 0.41E - 20.0$	TxN	Max. air temp (Nov)[b]	°C	0.002	0.39
				E	East = sin(aspect)	radians	0.021	0.26
	d-excess	Snow	$0.0042Elev - 0.010rM + 0.14$	Elev	Elevation	m	0.000	0.38
				rM	Short wave rad. (Mar)[b]	W/m^2	0.001	0.26

Note: Precipitation values rely on observed weather station data located near the sample location. Snowpit isotopic values rely on hydrologic model output at a given snowpit location.
Abbreviations: Mar, March; Nov, November.
[a]Mean daily.
[b]Mean monthly.

distributed as either snowfall or rain using techniques presented in previous work (Carroll et al., 2019, 2020) with an example provided in Figure 1b. Additional details on model parameterization, calibration and performance are given in the supporting information (SI).

4 | RESULTS

4.1 | Precipitation

Precipitation at RC exhibited a bi-modal distribution with winter snowfall ($\delta^{18}O = -17.6 \pm 5.2‰$; $\delta^{2}H = -126.5 \pm 43.0‰$; d-excess = 14.4 ± 5.0 ‰) and summer rains ($\delta^{18}O = -8.0 \pm 4.4‰$; $\delta^{2}H = -57.7 \pm 31.3‰$; d-excess = 6.3 ± 9.5‰) describing seasonal isotopic means. It is acknowledged the event sampling strategy did not aggregate across storm totals and data has the potential to exhibit scatter. This was especially apparent with monsoon rain in the summer and fall. As an example, on 9 September 2014, a single rainstorm was sampled at 1–3-h intervals. Observed intra-storm variability equalled 3.3‰ ($\delta^{18}O$), 28.4‰ ($\delta^{2}H$) and 12.0‰ (d-excess). These ranges are representative of single-storm events presented by others (Han et al., 2020). Despite the scatter in observations, the LMWL is well described by the least squares regression, $\delta^{2}H = 7.4\delta^{18}O + 2.4$ ($r^2 = 0.98$, $p \ll 0.001$). Disaggregating by precipitation phase produces a slope for snow ~8.0, while the slope for summer rain is shallower (~7.0).

Atmospheric variables correlated with precipitation isotopic content were assessed independently for rain and snow with the multiple linear regression models given in Table 1. Snowfall $\delta^{18}O$ was directly related to air temperature. Rain $\delta^{18}O$ also covaried directly with air temperature, with a direct relationship to wind speed providing additional information to improve statistical performance. Relative humidity was the primary predictor of d-excess in rain with low relative humidity lowering rain d-excess. Air temperature was a secondary variable that was indirectly related. Temporal plots of observed and predicted precipitation isotopes are provided in Figure 2. A linear lapse rate for $\delta^{18}O$ was calculated from average weekly aggregated snowfall and equalled −0.16 ± 0.12‰ per 100-m gain in elevation.

4.2 | Snowpack isotopic variability at peak snow accumulation

The isotopic composition of individual snowpits near peak accumulation collected 2016–2019 plot on the dual isotope space with annual slopes ranging from 7.0 to 7.9, and across all years was 7.3. Averaged annually, observed snowpit $\delta^{18}O$ means display similarity between years (Figure 2c) with annual differences correlated to winter temperature ($r^2 = 0.89$, $p = 0.06$). The average annual enrichment in snowpack compared to snowfall was small (0.22 ± 0.40‰), with more enrichment in snowpack occurring in years when March was warm ($r^2 = 0.80$, $p = 0.10$). In contrast, average annual d-excess in the snowpack was significantly lower than estimated snowfall for all years (−2.6 ± 1.0‰) (Figure 2d) with relative declines in average annual snowpack d-excess explained ($r^2 = 0.99$) by years with warmer temperatures in early winter ($p = 0.04$) and those years with higher solar radiation ($p = 0.02$). Spatial variability in observed $\delta^{18}O$ of individual snowpits was directly related to early winter air temperature ($p < 0.01$) and eastern aspect ($p = 0.02$). The estimated fraction of rainfall compared to total precipitation prior to 1 April increased snowpack $\delta^{18}O$ ($p < 0.01$) but did not add additional information to the multiple regression. Correlation statistics indicate the snowpack was more depleted in the northern and western regions of the ER domain and was more enriched where dense conifer forests reside. However, these correlations were weak in comparison to temperature and aspect. No relationship was observed between snowpit $\delta^{18}O$ and elevation. Observed d-excess in snowpits decreased ($r^2 = 0.46$) where or when March solar radiation was large ($p \ll 0.01$) and at lower

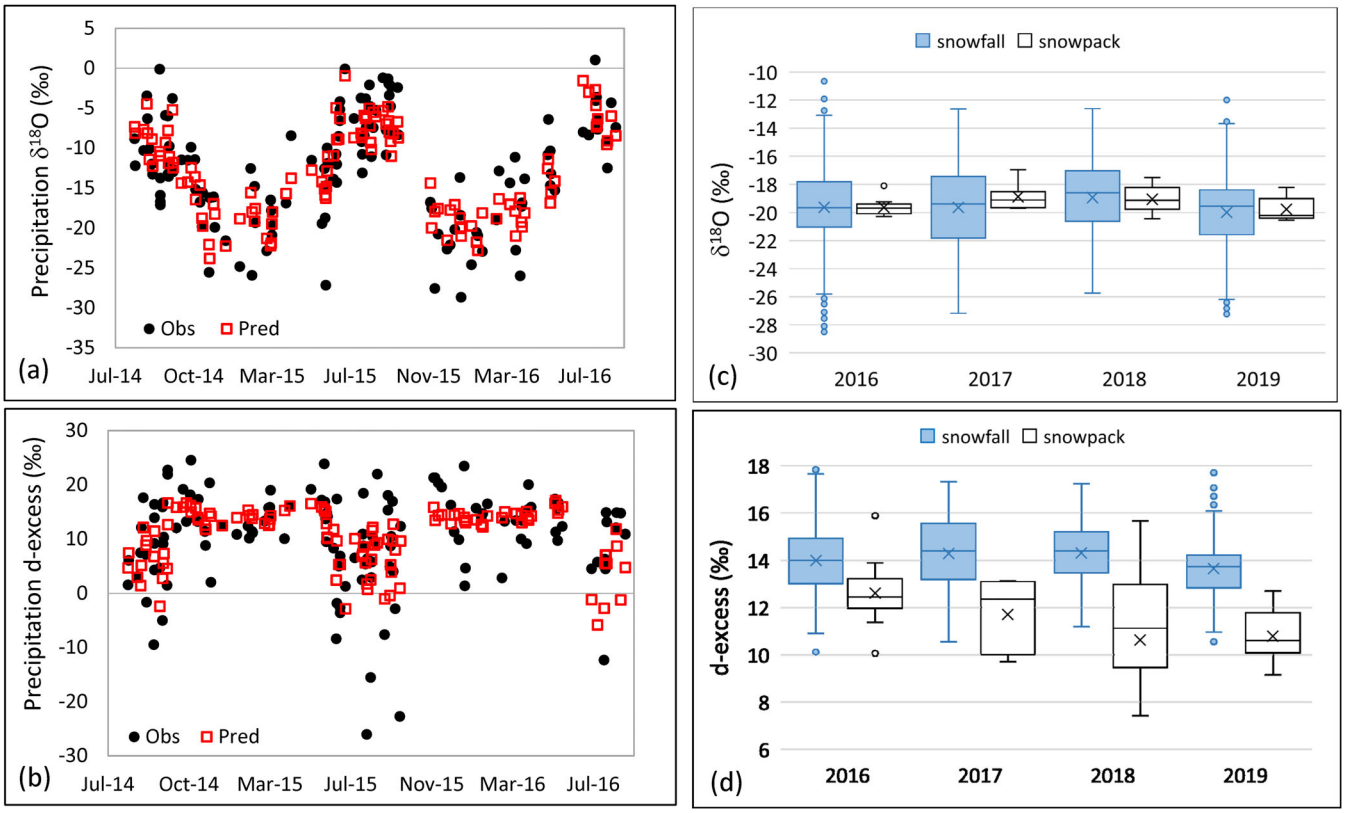

FIGURE 2 Observed versus predicted precipitation inputs at the RC site for (a) $\delta^{18}O$ and (b) d-excess. Precipitation includes both snow and rain. A comparison of annually averaged isotopic values for winter snowfall and snowpack at sample locations during peak snow water equivalent for (c) $\delta^{18}O$ and (d) d-excess. × = mean value

elevations ($p \ll 0.01$). The final spatial regression models for snowpack $\delta^{18}O$ and d-excess near peak accumulation are given in Table 1.

Snowpack isotopic observations with depth for individual sampling locations are provided in Figure 3. Depths are normalized by maximum SWE at 10% increments. In general, at the bottom of the snowpack $\delta^{18}O$ is relatively high compared to the annually averaged basin-wide snowpack mean. Snowpack $\delta^{18}O$ then decreases compared to the mean value in the middle of the snowpack (zone of depletion) and moves toward higher values at the top of the snowpack. Snowpack d-excess tends to decline from the bottom of the snowpack to the top. Deviations from the annual snowpack mean across the depth of the snowpack are best predicted by a direct relationship to maximum daily air temperature ($p < 0.05$ for all years) at the time of snowfall deposition. D-excess in snowpack layers showed no significant trend with daily air temperature, except during 2018 when winter conditions were warmer and drier (Figure 3l). Decreased relative humidity, increased wind speed, and increased solar radiation tend to increase $\delta^{18}O$ and decrease d-excess in snowpack layers. However, results were not consistently significant across all years at the basin-scale. Number of days of continuous precipitation and its inverse, the lack of precipitation, were also not significant predictors of average annual isotopic variability with snowpack depth.

Observed isotopic ratios in snowpack as function of depth were compared to estimated snowfall inputs from the land-surface model at individual snowpit locations. This was done to explore the potential for post-depositional changes to isotopes in the snowpack. An example is provided in Figure 4a,b. On average, snowfall $\delta^{18}O$ was estimated lower than snowpack $\delta^{18}O$, and snowfall d-excess was higher than snowpack d-excess, in the top quarter of the snowpack (25 ± 14% normalized by maximum SWE). Depths of snowfall bias increased as functions of maximum winter air temperature ($r^2 = 0.24$, $p = \ll 0.01$, Figure 4c) and lower total winter precipitation ($r^2 = 0.23$, $p \ll 0.01$, Figure 4d). Notably, snowpack $\delta^{18}O$ estimates are consistently more enriched (1.6 ± 1.2‰) and more depleted (1.7 ± 1.2‰) in the top 40% and lower 60% than the corresponding snowfall, respectively.

4.3 | Snowpack and snowmelt isotopic evolution over time

SWE at IRN (3191 m) and GTH (2926 m) tracked 2020 winter conditions at the Schofield and Butte SNOTEL, respectively (Figure 5). Intermittent periods of no snow were coincident with higher daytime temperatures, lower relative humidity, and higher solar radiation. Wind speed anomalies tended to be highest during precipitation events but were not isolated to snowstorms. The largest wind speeds began in late March and remained above the winter average through most of the spring. Detailed snowpit data for 2020 are given in Figure 6. Snowpack temperatures were coldest near the surface and increased with depth

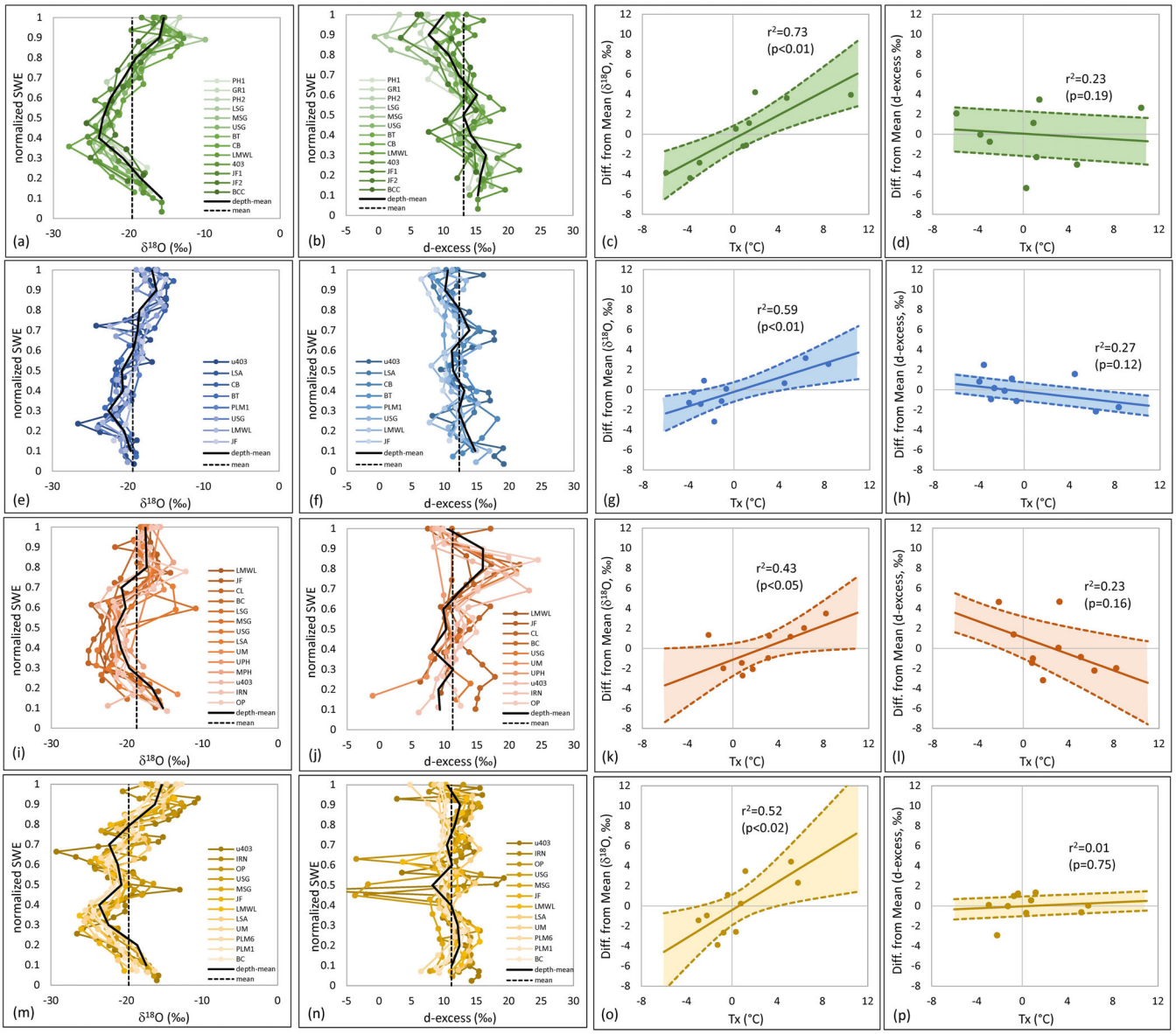

FIGURE 3 Snowpit observations across years as a function of normalized snow water equivalent (SWE): 2016 (a) $\delta^{18}O$, (b) d-excess and deviation from annual mean from the depth-mean as a function maximum daily temperature at the Schofield SNOTEL (Tx) (c) $\delta^{18}O$, (d) d-excess; 2017 (e) $\delta^{18}O$, (f) d-excess and deviation from annual mean (g) $\delta^{18}O$, (h) d-excess; 2018 (i) $\delta^{18}O$, (j) d-excess and deviation from annual mean (k) $\delta^{18}O$, (l) d-excess; 2019 (m) $\delta^{18}O$, (n) d-excess and deviation from annual mean (o) $\delta^{18}O$, (p) d-excess. Shaded areas are 90% confidence intervals

to approximately 0°C at the ground surface. Over time, the snowpits warmed and became isothermal when minimum daily air temperatures exceeded 0°C. Isothermal conditions occurred 3 weeks earlier at the GTH site (4 April) in comparison to the IRN site (28 April). Once isothermal, snow mass declined rapidly. During the accumulation phase, SWE at 10-cm increments tended to increase with depth and over time. Both indicating snowpack compaction and densification of deeper layers with added snow. The exception was the base (<30 cm) of the snowpack at IRN where lower density depth hoar resided and persisted into April. Higher $\delta^{18}O$ occurred immediately above these basal layers. In contrast, the GTH site did not exhibit a significant drop in snow density at its base, nor did these layers contain a relatively higher $\delta^{18}O$ content. Both snowpits experienced similar oscillating behaviour with $\delta^{18}O$ ranging between −25‰ and −15‰. The variability was largely maintained throughout the winter season. Once melting began, the snow layers were compressed and moved toward a relatively more enriched signature.

With respect to d-excess, the IRN snowpit contained greater variability than the GTH site. However, consistent trends did occur at both locations and across sample dates. At the base of the snowpack (<20–30 cm), lower d-excess occurred in comparison to the snowpack in the 40–70 cm above it. At (or near) the snowpack surface there tended to be a drop in d-excess that periodically could be overlain by snow layers of higher d-excess value. With

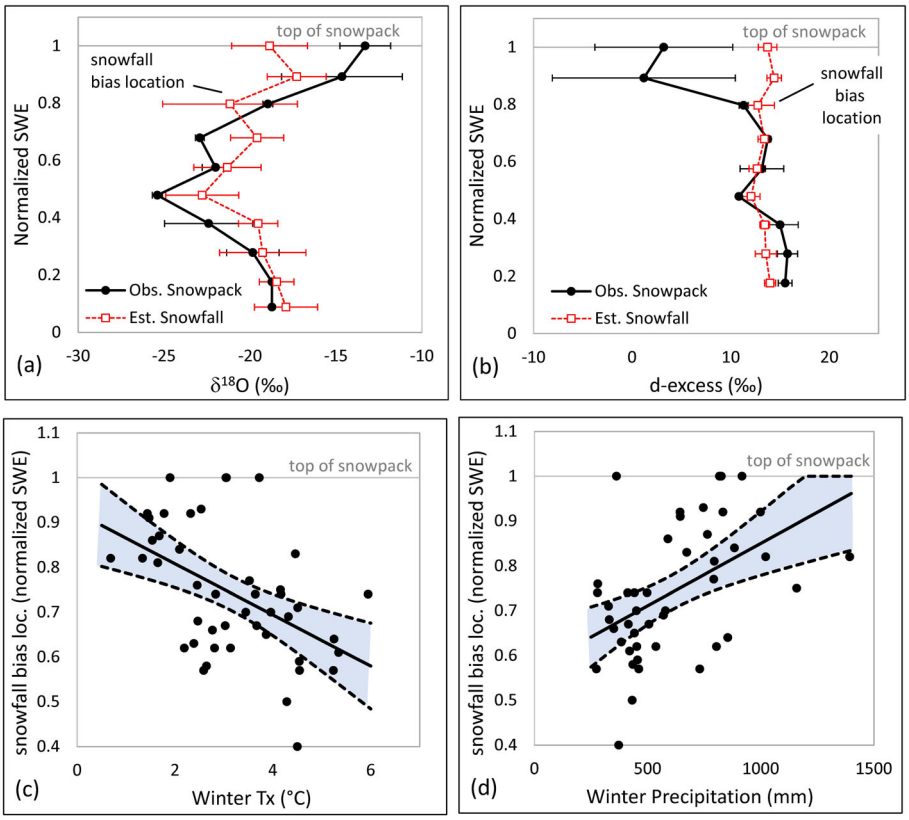

FIGURE 4 Example of estimated snowfall and observed snowpack (a) $\delta^{18}O$ and (b) d-excess for the 2016 snowpit PH2. Data are plotted across the snowpit height given as a normalized snow water equivalent (SWE). Snowfall bias location identified where snowpack observations shift away from snowfall estimates. Snowfall bias location for all snowpits compared to (c) average winter maximum daily air temperature, Tx and (d) and total winter precipitation for plot location. Shaded areas are 90% confidence intervals

snowmelt, snow layers and their d-excess values compressed. A dramatic shift toward a much lower d-excess value occurred in May at both locations following either a substantive dry period (GTH) and/or rain event (IRN).

Snowpit isotopic heat maps are provided in Figure 7 as an alternative visual to track isotopic evolution across snowpack layers at both sites. Blue (red) indicates relative decrease (increase) in $\delta^{18}O$ or increase (decrease) in d-excess in comparison to the combined snowpit mean. Memory of inter-storm variability appears largely maintained until late April at IRN, and March at GTH. After which snowpack enrichment and homogenization in $\delta^{18}O$ began at the top of the snowpack and rapidly extended across the snow column with progressive snow loss. Low d-excess occurred at the top of the snowpack at both locations in late January. At IRN, low d-excess layers were then buried by newer snowpack with higher d-excess. At the GTH site, lower d-excess values appear to accumulate at the snowpack surface and extend to 40% snowpack depth despite the addition of new snow. Correlation analysis indicates that d-excess declined in the top 10-cm of the snowpack at both IRN and GTH coincident with lower relative humidity, higher wind speed, higher solar radiation, and higher air temperature as defined by the climate 3-days prior to sample collection.

Figure 8a indicates bulk snowpack observations at GTH were lower in $\delta^{18}O$ than the higher elevation snowpack at IRN but enriched three-times more quickly over time as illustrated by a steeper slope. With the higher rate of enrichment, the lower elevation snowpack $\delta^{18}O$ became similar to the higher elevation snowpack in early April. Increase in snowpack $\delta^{18}O$ at IRN was 1.8‰ over the sampling period, and at GTH was 3.2‰. Enrichment during the ablation period from early April to total snow loss indicates the IRN site enriched 1.04‰ and the GTH site 1.36‰. The difference in snowpack isotopic values between sites equalled −0.16‰ per 100 m elevation, or the observed precipitation lapse rate. Figure 8b shows bulk snowpack d-excess at both locations was approximately 14‰ in the winter, with IRN showing no significant trend in d-excess over time. In contrast, the GTH snowpack averaged −0.02‰ per day change in d-excess and was significantly different from the higher elevation site by mid-March.

The rate of snowmelt $\delta^{18}O$ enrichment at higher elevation BT site was 0.04 ‰ per day with total enrichment equal to 0.6‰ from melt onset to completion (Figure 8c). At the lower elevation PLM1 site, snowmelt enrichment was three-times faster at 0.12‰ per day with total snowmelt enrichment equal to 5.5‰. Snowmelt d-excess decreased over time at both locations. The rate of decline at BT was −0.07‰ per day, while PLM experienced a rate of d-excess decline at −0.13 ‰ per day (Figure 8d). Normalized over elevation, snowmelt $\delta^{18}O$ increased, and d-excess decreased approximately 0.02‰ per day per 100-m elevation lost.

5 | DISCUSSION

5.1 | Isotopic composition of precipitation

Precipitation isotopic content must be defined to establish the influence of snow and rainfall inputs on snowpack isotopic evolution.

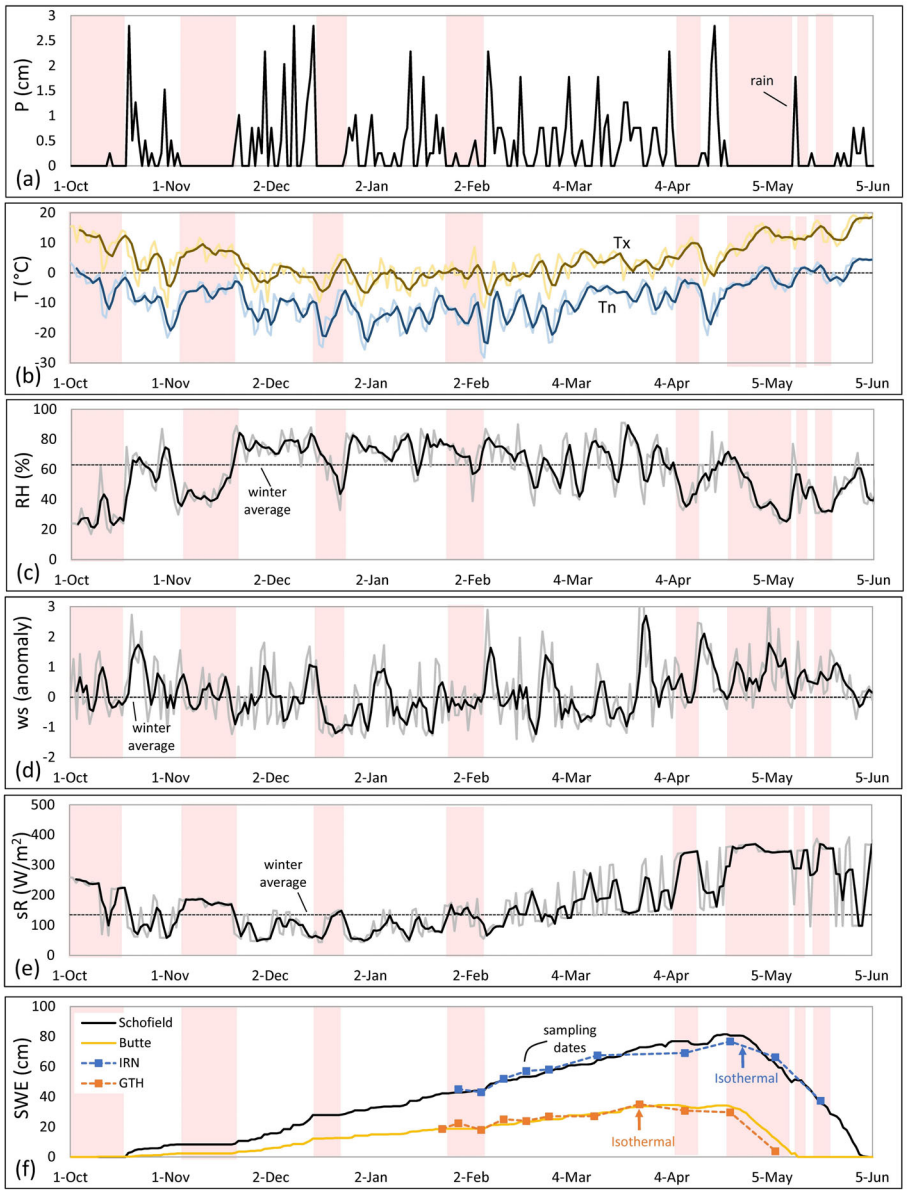

FIGURE 5 Daily 2020 conditions at the Schofield SNOTEL (a) precipitation, (b) temperature (Tx = maximum, Tn = minimum); and KCOMTRE2 station (c) relative humidity, (d) wind speed anomaly, (e) estimated solar radiation. Dark lines = 3-day average. (f) A comparison of snow water equivalent between SNOTEL (solid lines) and isotopic sampling locations (dashed). Shaded areas are periods of low/no precipitation

Putman et al. (2019) found LMWLs are not well defined with less than 4 years of data. We base our LMWL calculation on only 2 years of data, but the large number of observations linearly aligned with a high degree of correlation in the dual isotope space and our LMWL is in agreement with previous sampling campaigns in the region (Marchetti & Marchetti, 2019). The ER LMWL contains a slightly reduced slope in comparison to the GMWL, but when divided into rain and snow illustrates fundamental differences between warm and cold season precipitation. Snowfall originates from northwest frontal storms (Marchetti & Marchetti, 2019) and contains low isotopic values due to cold, high elevation conditions with a low vapour fraction (Dansgaard, 1964). Snowfall resides on the GMWL with d-excess values ≥10‰ indicating a low potential for evaporation. Similar to Otte et al. (2017), the oxygen isotopic composition of precipitation is correlated to ambient air temperature and the phase of precipitation. These are common proxies for the Rayleigh distillation effect as storms move inland, and reflect differences between the temperature of the initial cloud condensate in the air mass and the condensation temperature at our sampling site (Beria et al., 2018; Clark & Fritz, 1997; Putman et al., 2017). The slope describing $\delta^{18}O$ in snow as a function of temperature is 0.6‰ per °C which falls in the range presented by others (Bowen, 2008; Marchetti & Marchetti, 2019) and deemed acceptable.

In contrast to snow, summer rains in the ER originate from monsoon surges of tropical atmospheric moisture with local convective precipitation occurring in the afternoons (Marchetti & Marchetti, 2019). Summer months experience more recycling of moisture via evaporation than winter precipitation as storms move inland from the ocean. Consequently, rainfall produces more enriched conditions and a larger decrease in d-excess for a given increase in temperature than snow. Temperature remains an important descriptor of stable water isotopes in rain but isotopic content is modified by

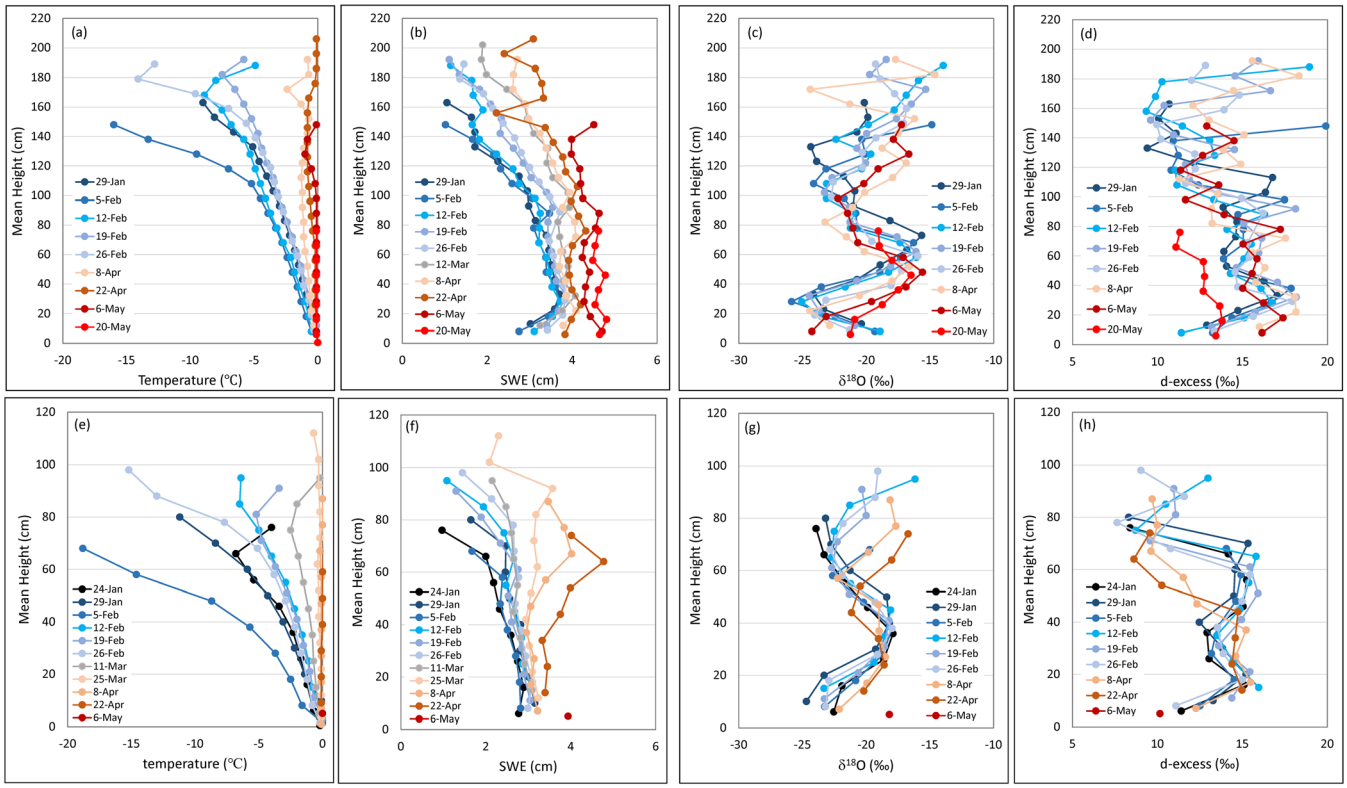

FIGURE 6 2020 snowpit observation across snowpack height for IRN (a) temperature, (b) snow water equivalent, SWE, (c) $\delta^{18}O$, (d) d-excess; and GTH (e) temperature, (f) SWE, (g) $\delta^{18}O$, (h) d-excess

(a)

Snowpack Height (cm)	24-Jan	29-Jan	5-Feb	12-Feb	19-Feb	26-Feb	12-Mar	8-Apr	22-Apr	6-May	20-May
210	No Data						-16.30		-15.57		
200					-18.44		-16.89	-17.70	-16.52		
190				-14.66	-19.74	-19.14	-17.28	-14.62	-15.63		
180				-15.91	-15.34	-19.47	-17.87	-24.40	-16.18		
170		-20.16		-16.86	-16.47	-18.46	-15.77	-21.30	-23.43		
160		-19.87		-17.80	-17.63	-17.23	-16.23	-16.21	-17.47		
150		-20.74	-14.86	-19.85	-19.98	-16.24	-17.77	-17.51	-16.47	-17.24	
140		-24.35	-20.36	-22.38	-20.74	-17.87	-20.18	-18.75	-18.00	-17.87	
130		-23.90	-20.08	-19.65	-20.06	-20.70	-20.24	-16.86	-17.13	-16.66	
120		-21.78	-23.16	-20.37	-22.69	-19.76	-23.09	-17.93	-16.94	-19.07	
110		-20.91	-24.13	-23.12	-23.28	-21.13	-21.82	-20.14	-19.65	-20.19	
100		-21.03	-21.74	-23.13	-21.34	-23.79	-20.70	-21.07	-20.33	-22.23	
90		-18.15	-20.83	-21.03	-21.28	-21.65	-20.10	-23.24	-22.87	-21.47	
80		-15.66	-20.70	-21.25	-17.59	-21.13	-16.96	-21.57	-21.38	-21.06	-19.06
70		-16.82	-16.29	-17.36	-16.09	-19.57	-15.90	-20.15	-20.62	-20.66	-18.98
60		-18.91	-17.30	-16.09	-18.10	-15.95	-17.83	-16.60	-16.95	-17.11	-17.99
50		-20.74	-18.95	-18.25	-20.74	-17.24	-20.66	-17.97	-16.52	-15.59	-16.49
40		-24.14	-23.54	-21.66	-24.48	-18.05	-24.63	-20.54	-18.82	-16.89	-17.49
30		-23.35	-25.86	-25.07	-23.71	-23.17	-21.46	-24.44	-22.95	-19.59	-18.75
20		-20.39	-22.43	-23.52	-20.90	-24.04	-18.79	-22.89	-23.66	-23.15	-20.92
10				-18.91		-21.31			-21.48	-24.28	-21.25
mean		-20.72	-20.54	-19.95	-20.08	-20.05	-19.34	-19.94	-19.23	-19.66	-18.89

(c)

Snowpack Height (cm)	24-Jan	29-Jan	5-Feb	12-Feb	19-Feb	26-Feb	12-Mar	8-Apr	22-Apr	6-May	20-May
210	No Data						No Data		12.6		
200					15.9			15.6	13.7		
190				14.5	14.6	12.9		18.3	15.1		
180				10.2	16.6	12.0		14.5	16.5		
170		10.7		9.9	10.4	12.5		12.1	11.6		
160		10.0		9.3	9.6	17.0		13.0	12.1		
150		11.1	19.9	11.4	10.9	10.5		15.1	13.8	12.9	
140		9.4	10.9	13.1	14.5	9.5		13.9	13.1	14.5	
130		12.1	11.2	13.4	11.6	11.1		14.9	14.5	12.7	
120		16.8	10.8	11.1	11.8	13.0		11.3	11.1	11.4	
110		16.4	12.4	11.1	13.6	11.6		13.5	11.8	13.6	
100		13.9	17.5	13.3	18.1	12.2		13.2	12.5	11.6	
90		14.7	14.7	16.3	15.1	17.3		13.2	12.0	13.9	
80		14.6	15.0	14.1	16.2	15.0		17.5	16.6	17.2	11.3
70		13.9	15.0	15.5	15.9	15.3		15.6	14.9	15.0	11.1
60		14.1	13.9	15.1	14.7	15.4		16.3	15.7	15.9	11.7
50		16.3	14.3	14.3	17.1	14.6		15.8	15.5	15.6	12.1
40		17.0	17.9	16.1	18.2	14.7		18.1	15.6	15.0	12.8
30		14.7	16.6	16.7	15.7	17.9		18.1	17.7	16.2	13.3
20		12.9	14.4	15.1	13.2	15.6		16.0	15.7	17.4	13.2
10				11.4		13.3			14.0	16.2	13.5
mean		14.60	14.69	13.59	14.46	14.13		15.12	14.43	14.45	12.66

(b)

Snowpack Height (cm)	24-Jan	29-Jan	5-Feb	12-Feb	19-Feb	26-Feb	12-Mar	8-Apr	22-Apr	6-May	20-May
120							No Data				No Snow
110											
100				-16.17	-20.34	-19.09					
90				-21.28	-20.00	-19.30		-18.12			
80	-23.93	-23.18		-22.51	-22.28	-21.82		-17.67	-16.71		
70	-23.30	-22.77	-19.72	-22.72	-22.70	-22.82		-19.82	-17.99		
60	-21.76	-21.26	-22.63	-21.23	-21.33	-21.88		-22.24	-20.47		
50	-19.88	-18.39	-20.21	-18.08	-18.21	-19.30		-19.01	-21.15		
40	-17.90	-18.18	-17.98	-18.52	-18.56	-17.96		-18.98	-19.03		
30	-18.62	-19.25	-18.68	-19.39	-20.62	-19.12		-18.48	-18.59		
20	-21.90	-23.30	-20.82	-23.31	-23.28	-22.93		-19.93	-20.18		
10	-22.54	-24.69	-23.26			-23.19		-22.11		-18.27	
mean	-20.96	-21.45	-20.60	-20.78	-20.97	-21.03		-19.63	-19.14	-18.27	

(d)

Snowpack Height (cm)	24-Jan	29-Jan	5-Feb	12-Feb	19-Feb	26-Feb	12-Mar	8-Apr	22-Apr	6-May	20-May
120	No Data						No Data				No Snow
110											
100				12.98	10.97	9.04					
90				10.50	11.08	11.59		9.70			
80	8.39	8.31		8.72	9.58	7.63		9.99	9.56		
70	14.18	15.34	14.06	15.81	15.46	10.78		9.62	8.62		
60	15.26	14.58	14.93	15.38	15.93	15.46		11.53	10.26		
50	15.05	14.50	14.63	14.87	14.96	14.99		12.34	14.75		
40	12.93	12.48	13.53	13.51	13.61	13.55		15.22	14.59		
30	13.05	13.84	13.19	14.45	15.44	13.88		14.61	14.40		
20	15.11	15.22	14.52	15.97	14.39	15.01		15.49	14.98		
10	11.41	13.28	12.51			11.10		12.27		10.32	
mean	13.62	13.87	13.86	13.93	13.74	12.60		12.12	12.38	10.32	

FIGURE 7 Heat maps for 2020 snowpits. Higher (blue) and lower (red) $\delta^{18}O$ as a function of snowpack height for (a) IRN, elevation 3191 m, and (b) GTH, elevation 2926 m. Higher (blue) and lower (red) d-excess as a function of snowpack height for (c) IRN and (d) GTH. Snowpack height rounded to the nearest 10 cm

kinetic effects of high wind and low relative humidity (Clark & Fritz, 1997; Kopec et al., 2019). Despite statistical significance, there is a large amount of scatter in the linear regressions describing observed precipitation isotopic inputs using on-site climate data, and regressions fail to capture the observed distribution endmembers. Inability to estimate endmembers is likely due to a sampling strategy

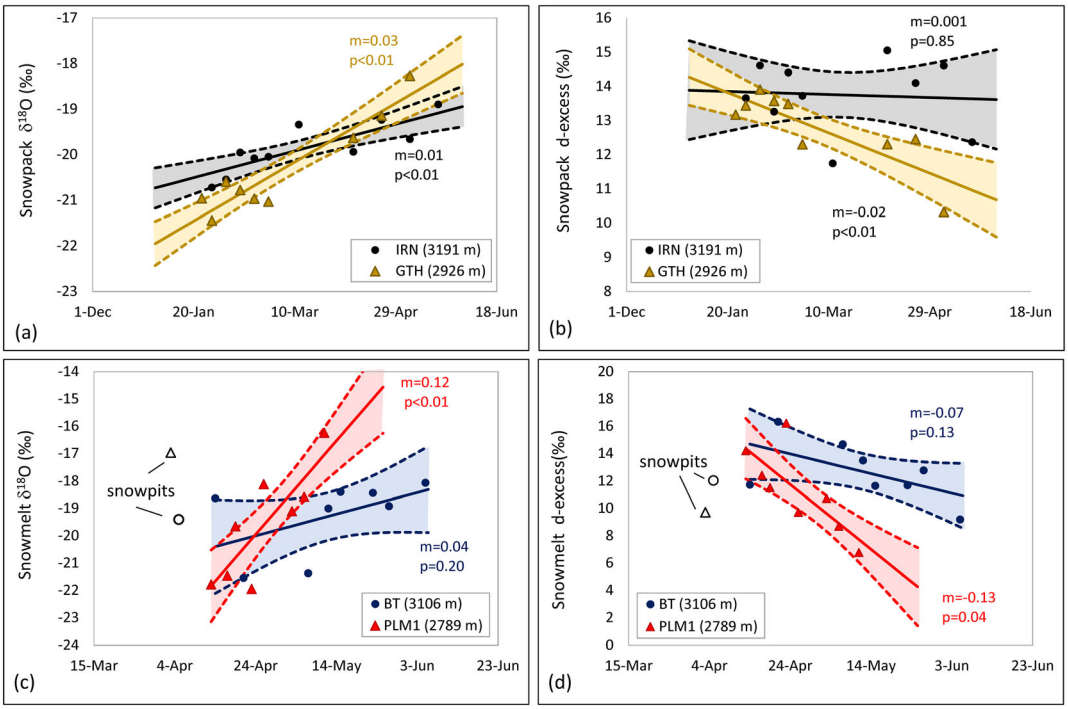

FIGURE 8 SWE-weighted snowpack observations in 2020 for (a) $\delta^{18}O$ and (b) d-excess. Snowmelt collected in 2017 for (c) $\delta^{18}O$ and (d) d-excess. Snowpit values near peak SWE provided (BT based on 2016 data). Slopes (m) for regressions provided as ‰ per day. Shaded areas are 80% confidence intervals

that failed to capture sub-storm variability associated with the frontal passage of storms. It is also likely that local climate fails to represent mechanisms such as sub-cloud evaporation and mixed-phase cloud processes (Putman et al., 2019). Despite these limitations, the regression models capture the majority of isotopic behaviour in precipitation using a simple approach and allows us to define individual storms across the period of snowpack analysis.

5.2 | Spatial distribution of $\delta^{18}O$ in snowpack at peak snow accumulation

We observed that snowpack largely preserved precipitation $\delta^{18}O$ inputs across all scales of analysis. This is consistent with prior studies (Clark et al., 1970; Dahlke & Lyon, 2013; Hürkamp et al., 2019; Stichler et al., 1981; Unnikrishna et al., 2002). Given air temperature is the defining predictor variable for snowfall $\delta^{18}O$, it is not unexpected that air temperature is the most important predictor for $\delta^{18}O$ in snowpack. Aspect emerged as a secondary control on snowpack isotopic content. Dahlke and Lyon (2013) recognized the influence of aspect, via the direct impacts of solar radiation, where sunnier aspects tend to hold isotopically heavier snow. Our results are contradictory, with data showing snowpack more enriched along the topographically shaded eastern aspects and, to a lesser degree, along the northern aspects. North and east aspects are notorious in the Rocky Mountains for preserving early snowfall. This snowfall is subjected to loss of crystalline structure (depth hoar) at the base of the snowpack that enhances avalanche risk (refer to http://www.cbavalanchecenter.org; Johnson & Jamienson, 2000). The formation of depth hoar is caused by temperature-gradient induced vapour diffusion through the snowpack. The preservation of early snowfall and resulting depth hoar enrich the snowpack in ^{18}O relative to its initial state in the bottom 10–20 cm of the snowpack (Friedman et al., 1991; Zhang et al., 1996). In addition, wind scoured snow preferentially deposits along north-east aspects in the ER (Carroll et al., 2019). Wind promotes sublimation through either saltation (Essery et al., 1999; Wang et al., 2019) or pressure pumping (Colbeck, 1989) with the potential to increase $\delta^{18}O$ on the snowpack surface. Data suggest the net effect of isotopic enrichment via vapour loss preserved at either at the base or surface of the snowpack is substantial enough to affect bulk snowpack $\delta^{18}O$ signatures along north-east aspects when sampled at peak accumulation.

Several parameters showed lack of correlation to snowpack $\delta^{18}O$. Observed spatial variability in snowpack $\delta^{18}O$ indicates slightly higher values in dense canopy forests. Isotopically enriched throughfall has been observed in other studies with enrichment increasing for smaller snow particles, denser canopy cover, longer residence times of storage and under clear-sky conditions (Claassen & Downey, 1995; Koeniger et al., 2008). However, the relationship was not statistically significant in the ER and was discarded as first-order control. Elevation was similarly found to have no descriptive ability for snowpack $\delta^{18}O$ at peak accumulation. To mimic the lack of observed trend in

snowpack across elevation, $\delta^{18}O$ in snowfall must implicitly account for elevation through use of the observed precipitation lapse rate of −0.16‰ per 100-m. The observed lapse rate approximates other studies in North America (−0.17‰–0.22‰, Friedman et al., 1992; Tappa et al., 2016) and is considered reasonable. With no isotopic lapse rate in precipitation, the estimated $\delta^{18}O$ signature in snowpack at peak SWE is estimated relatively too enriched at higher elevation and too depleted at low elevation compared to the observed. Including the lapse rate offsets the preservation of early winter snowfall that is seasonally more enriched at higher elevations, and the influence of vapour loss on isotopic content of this persistent early snowpack. At lower elevations, early season snowfall is largely ephemeral and does not contribute to bulk snowpack isotopic content. With the delay in snowpack accumulation at lower elevations, the snowpack begins with lower $\delta^{18}O$ values in comparison to higher elevation snowpack (e.g., Figure 8a). Inclusion of the precipitation isotopic lapse rate allows a faster rate of enrichment over time in the lower elevation snowpack compared to higher elevations. By peak accumulation, snowpack $\delta^{18}O$ is effectively similar across elevation gradients. This is discussed further in Section 5.4.

5.3 | Post-depositional change in snowpack at peak snow accumulation

Stable water isotopes in snowpack can provide context of where and when melt-freeze processes have begun and where water vapour loss may be critical to the water balance of the snowpack. There is some evidence of post-depositional change in snowpack using $\delta^{18}O$ observations. For example, reduced interannual variability in snowpack in comparison to estimated snowfall from the land-surface model (Figure 2c) could be attributed to isotopic redistribution and enrichment in the snowpack (Friedman et al., 1991; Taylor et al., 2001). This hypothesis is supported by the predictive power of late winter air temperatures to describe the enrichment in bulk snowpack compared to total snowfall both at the aggregated annual and individual sample location scales. Higher temperatures in late winter drive earlier onset of snowmelt, the isotopic homogenization of snowpack and loss of heavier isotopes.

However, the lack of statistical difference between average annual snowfall and snowpack $\delta^{18}O$ hints that isotopic mass loss was not a dominant process at the time of peak SWE for the sites sampled. Likewise, at the plot-scale, results indicate the potential for mass movement of lighter isotopes downward and accumulating in the lower portions of the snowpack, but that significant snow water loss via snowmelt was not definitive based on the $\delta^{18}O$ mass balance across the entire snow column. On average, the depth of possible mass movement via melt occurred in the top 25% of the snowpack but depths ranged from 0% to 60% from snowpack surface across all observed locations. The greatest depths of potential snowmelt percolation occurred where daytime temperatures were high, and snowpack was shallow. These statistical results are intuitive, given locations with warmer temperatures are known to accelerate isothermal conditions (Burns et al., 2014) to initiate melt; and for equal temperatures, shallower snowpack is expected to become isothermal more quickly than deeper snowpack.

Decreases in d-excess between snowfall inputs and observed snowpack can help isolate where and under what conditions or locations vapour losses from snowpack may be most important in the ER. At the annual scale, snowpack samples sit on the dual isotope space with slopes equal to 7.0–7.9. Slopes are below that of incoming snowfall (~8.0) and slope reductions are best predicted by high air temperatures, high solar radiation, and low winter precipitation. The plot-scale analysis also found reductions in d-excess were larger in comparison to snowfall inputs at lower elevations and where snow accumulation was low. The influence of vapour loss on snowpack d-excess is a balance between energy and snow availability. Large elevational gradients it the ER produce large gradients in aridity, with lower elevations having both lower precipitation and higher potential evapotranspiration (Carroll et al., 2020). Higher potential evapotranspiration can promote larger sublimation losses. If these losses occur where or when shallow snowpack exists, then vapour losses are a larger proportion of the snow budget and d-excess declines in snowpack become more prominent. Likewise, Sexstone et al. (2018) found a larger proportion of the snowpack water budget was lost to sublimation when winter snowpack was low.

Attempts to tease out the effects of increased temperature on raising d-excess in new snowfall (refer to Table 1) compared to decreases in d-excess in the snowpack from vapour loss when snowfall did not occur, were largely inconclusive at the basin-scale. Specifically, the relationship of annually averaged d-excess with depth in the snowpack to air temperature was statistically muted (Figure 3). The muted response to temperature across most years could be due to either limited sublimation in the basin (Schlaepfer et al., 2014) or the condensation of night-time vapour that compensates for any day time enrichment (Beria et al., 2018; Stichler et al., 2001) such that changes in d-excess are not apparent at this aggregated scale. The exception was 2018 (Figure 3l). The winter of 2018 was very dry and warm and d-excess declines in snowpack layers occurred globally across the sampled locations as a function of temperature. Refining the resolution from basin-scale assessment of snowpack layers to that of individual snowpits, we find that the depth of d-excess declines in snowpack was correlated to both higher daytime temperatures and shallower snowpack that was not generally apparent at the basin-scale. This indicates that d-excess declines in the snowpack are primarily influenced by landscape position dictating the relationship between atmospheric demand and depth of snowpack and secondarily by annual climate conditions.

5.4 | Snowpack and snowmelt isotopic evolution over time

The detailed depth-dependent $\delta^{18}O$ observations at the IRN and GTH sites help provide context and validation of the spatially extensive data collected at peak SWE. First, individual snow events were largely

preserved in the snowpack. Snow layers alternated between periods of relatively high and low $\delta^{18}O$, as defined by storm variability, that was consistent between sites and across time until the snowpack became isothermal and homogenized. Despite isotopic memory in the snowpack, the bulk isotopic values evolved differently across sites. Specifically in January, the lower elevation GTH snowpack $\delta^{18}O$ was observed 1.3‰ lower than expected in comparison to the IRN site based on elevational differences and the observed precipitation lapse rate. This discrepancy may be related to the earlier onset of snowpack accumulation at IRN (Figure 5f), its corresponding seasonally enriched snowfall, as well as the observed development of low-density depth hoar and associated $\delta^{18}O$ increase at the base of the snowpack. As discussed previously, this is analogous of the persistence of early snowfall along north-east aspects that we hypothesized may have imposed higher $\delta^{18}O$ in bulk snowpack within the ER. In addition, the delayed snow accumulation at the GTH site, and a lack of low density and high $\delta^{18}O$ observed at the base of the GTH snowpit are partly responsible for its initially depleted bulk signature.

While initially lower in $\delta^{18}O$, the GTH snowpack enriched three-times faster in comparison to the IRN site with differences in snowpack $\delta^{18}O$ enrichment approximately equal to the elevational lapse rate. The implication is that snowpack $\delta^{18}O$ enrichment over time was dominated by differences in mass loading from precipitation. The differing enrichment rates produce isotopically similar snowpack by peak SWE. This agrees with the multi-year spatial analysis at/near peak SWE that found no elevation control on snowpack $\delta^{18}O$. While elevation is not a good predictor of $\delta^{18}O$ in snowpack at peak accumulation, it is instrumental in defining snowpack $\delta^{18}O$ over time by describing snow presence or absence in the early season and the lapse rate of ^{18}O mass inputs.

D-excess in snowpack also appears to evolve differentially across elevation. In January, the two locations were similar with respect to bulk d-excess values. Over time, the higher elevation site showed large variability but no significant trend in d-excess, while the lower elevation site experienced a net decline. Previous research indicates that sublimation tends to increase as a result of low atmospheric pressure, low humidity, increased solar radiation and high wind speeds (Earman et al., 2006; Stigter et al., 2018). Sublimation from spatially distributed wind or pressure fields (Colbeck, 1989) can enhance diffusion 8%–11% (Bowling & Massman, 2011) but these effects from wind shear are often limited in the top few centimetres of the snowpack (Clifton et al., 2008). Limiting our analysis to the upper-most sample (top 10-cm) we find that d-excess at both sites were correlated to lower relative humidity, higher wind speed, higher daytime temperature and higher solar radiation averaged over the 3 days prior to sample collection. Over the winter accumulation period, the vapour-altered surface snow becomes buried by new snow of higher d-excess. If depth of new snow is large and time in-between snowstorms is short, then sublimation of the new snowfall is limited, and the snowpack exhibits alternating layers of high- and-low d-excess. The IRN site displays this kind of high vertical variability and, as a result, has no significant trend with d-excess over time. At the lower elevation GTH site there are smaller incremental snow additions from fewer storms and a greater potential to accumulate and aggregate sublimation on each successive storm-event. The effect is to decrease d-excess at depth. This layering-hypothesis provides an explanation for kinetic fractionation extending deep into the snowpack despite sublimation assumed limited to the upper few centimetres of the snowpack. Aggregated d-excess declines at the snow surface are large enough in the shallow GTH snowpack to affect bulk snowpack composition with snowpack d-excess decreasing significantly over the winter season.

Unfortunately, snowmelt observations were not coincident with the detailed temporal snowpack observations in 2020. However, observed isotopic content in snowmelt followed well established trends with initial meltwater isotopically lower in $\delta^{18}O$ in comparison to snowpack and becoming progressively more enriched in heavier isotopes over time (Ala-aho et al., 2017; Beria et al., 2018; Taylor et al., 2001, 2002). Observed snowmelt (0.6‰–5.5‰) enrichment over time reflected observed ranges in other studies (Lee et al., 2010; Unnikrishna et al., 2002). However, at low elevation the total increase in $\delta^{18}O$ exceed estimates based on snowfall inputs alone. The year snowmelt was collected (2017) was much warmer than all other years in the study. We hypothesize rainfall, with higher $\delta^{18}O$ at a given temperature, occurred at lower elevations and was responsible for large isotopic enrichment observed in snowmelt. As an example, from Table 1, rainfall $\delta^{18}O$ at 0°C and assuming average wintertime relative humidity and wind speeds, produces a 4.3‰ increase over snowfall. The sharp decline in snowmelt d-excess at the PLM1 site also hints at rainfall supplementing snowmelt. Altitudinal effects related to isotopic mass inputs in precipitation and the phase shift from snow to rain, are believed to drive melt water enrichment, with empirical evidence suggesting $\delta^{18}O$ snowmelt enrichment equal to 0.02‰ per day per 100 m lost in elevation. Similarly, d-excess decreased 0.02‰ per day per 100 m lost in elevation.

6 | CONCLUSIONS

For decades, research has used stable water isotopes to explore hydrologic processes in snowmelt-dominated catchments. Watersheds reliant on snow water inputs alter the timing of water inputs through snow storage and may produce a different isotopic input signal as a function of post-depositional metamorphism in the snowpack. Our work builds on this long history of empirical studies by exploring snowpack isotopes over substantial gradients in topography and vegetation structure, and over a 5-year period in a headwater basin of the Colorado River. Observed snowfall isotopic inputs were strongly correlated to air temperature and plotted along the GMWL with d-excess values ≥10‰ indicative of a low potential for evaporation. Results suggest precipitation isotopic inputs adjusted by the observed $\delta^{18}O$ elevational lapse rate (−0.16‰ per day per 100 m) are the primary descriptors of the spatial distribution of snowpack isotopic content across the basin at peak accumulation. Aspect was a secondary

control, with north and east aspects having slightly more enriched snowpack prior to freshet melt compared to other aspect. This enrichment was likely due to preservation of seasonally enriched snowfall in the early winter, the formation of isotopically light depth-hoar that persisted at the base of the snowpack, and wind effects that promoted enrichment at the top of the snowpack. Sublimation, as expressed by decreased d-excess in comparison to snowfall contributions, was highest at lower elevations and when/where temperatures and solar radiation were high. Evidence suggests the depth of post-depositional metamorphism (melt and vapour loss) occurred in the top 25% (range 0%–60%) of the snowpack with depths increasing at low elevation and where snowpack was shallow. Total depth of sublimation in the snowpack was likely the result of consecutive intermittent no-snow periods that aggregated over time, especially at lower elevations with low snowpack. Once minimum daily temperatures exceeded 0°C, the snowpack became isothermal followed by isotopic enrichment. Lower elevation snowpack and snowmelt experienced more rapid rates in enrichment over time. Results suggest enrichment rates over time were largely described by elevation. Elevation dictates early snow persistence or absence, isotopic lapse rates in precipitation and the phase shift of snow to rain. Hydrologic tracer studies using stable water isotopes in basins of large topographic relief, requires an adjustment for these elevational controls to properly constrain stream water sourcing from snowmelt.

ACKNOWLEDGEMENTS

Work was supported by the US Department of Energy Office of Science under contract DE-AC02-05CH11231 as part of Lawrence Berkeley National Laboratory Watershed Function Science Focus Area. We would like to express appreciation to the Rocky Mountain Biological Laboratory for handling Forest Service permitting. Synoptic field surveys were only possible with help from many people, including Torrey Carroll, Tony Brown, Lindsay and Adam Bearup, Laura Condon, Cheryl Cwelich, Amanda Henderson, Corey Lawrence, Helen Malenda, Katie Markovich, Anna and Josh Ryken.

DATA AVAILABILITY STATEMENT

Additional data and analysis are provided in the Supporting Information. Stable water isotopic data are available to the public at https://data.ess-dive.lbl.gov/view/doi:10.15485/1824223. The site RC in this manuscript is listed as LMWL in the published data set.

ORCID

Rosemary W. H. Carroll https://orcid.org/0000-0002-9302-8074
Jeffery Deems https://orcid.org/0000-0002-3265-8670
Reed Maxwell https://orcid.org/0000-0002-1364-4441
Matthias Sprenger https://orcid.org/0000-0003-1221-2767
Wendy Brown https://orcid.org/0000-0002-7237-1797
Alexander Newman https://orcid.org/0000-0002-1574-8754
Curtis Beutler https://orcid.org/0000-0003-0740-3112
Markus Bill https://orcid.org/0000-0001-7002-2174
Susan S. Hubbard https://orcid.org/0000-0003-2966-5631
Kenneth H. Williams https://orcid.org/0000-0002-3568-1155

REFERENCES

Ala-aho, P., Tetzlaff, D., McNamara, J. P., Laudon, H., Kormos, P., & Soulsby, C. (2017). Modeling the isotpic evolution of snowpack and snowmelt: Testing a spatially distributed parsimonious approach. *Water Resources Research*, *53*, 5813–5830. https://doi.org/10.1002/2017WR020650

Bales, R. C., Molotch, N. P., Painter, T. H., Dettinger, M. D., Rice, R., & Dozier, J. (2006). Mountain hydrology of the western United States. *Water Resources Research*, *42*(8), 1–13. https://doi.org/10.1029/2005WR004387

Barnett, T. P., Adam, J. C., & Lettenmaier, D. P. (2005). Potential impacts of a warming climate on water availability in snow-dominated regions. *Nature*, *438*, 303–309. https://doi.org/10.1038/nature04141

Bearup, L. A., Maxwell, R. M., Clow, D. W., & Mccray, J. E. (2014). Hydrological effects of forest transpiration loss in bark beetle-impacted watersheds. *Nature Climate Change*, *4*(6), 481–486. https://doi.org/10.1038/NCLIMATE2198

Beria, H., Larsen, J. R., Ceperley, N. C., Michelon, A., Vennemann, T., & Schaefli, B. (2018). Understanding snow hydrological processes through the lens of stable water isotopes. *Wiley Interdisciplinary Reviews: Water*, *5*(6), 1–23. https://doi.org/10.1002/wat2.1311

Berkelhammer, M., Still, C., Ritter, F., Winnick, M., Anderson, L., Carroll, R., Carbone, M., & Williams, K. H. (2020). Persistence and plasticity in conifer water-use strategies. *Journal of Geophysical Research: Biogeosciences*, *125*(2), 1–20. https://doi.org/10.1029/2018JG004845

Bowen, G. J. (2008). Spatial analysis of the intra-annual variation of precipitation isotope ratios and its climatological corollaries. *Journal of Geophysical Research*, *113*, D05113. https://doi.org/10.1029/2007JD009295

Bowen, G. J., Cai, Z., Fiorella, R. P., & Putman, A. L. (2019). Isotopes in the water cycle: Regional-to global-scale patterns and applications. *Annual Review of Earth and Planetary Sciences*, *47*, 453–479. https://doi.org/10.1146/annurev-earth-053018-060220

Bowling, D. R., & Massman, W. J. (2011). Persistent wind-induced enhancement of diffusive CO_2 transport in a mountain forest snowpack. *Journal of Geophysical Research: Biogeosciences*, *116*(4), 1–15. https://doi.org/10.1029/2011JG001722

Breckheimer, I. (2021). High resolution landcover maps for the upper Gunnison Basin derived from LiDAR and NAIP imagery. *Watershed Function Science Focus Area*. Written communication, April 5, 2021.

Broxton, P. D., Harpold, A. A., Biederman, J. A., Troch, P. A., Molotch, N. P., & Brooks, P. D. (2015). Quantifying the effects of vegetation structure on snow accumulation and ablation in mixed-conifer forests. *Ecohydrology*, *8*(6), 1073–1094. https://doi.org/10.1002/eco.1565

Burns, S. P., Molotch, N. P., Williams, M. W., Knowles, J. F., Seok, B., Monson, R. K., Turnipseed, A. A., & Blanken, P. D. (2014). Snow temperature changes within a seasonal snowpack and their relationship to turbulent fluxes of sensible and latent heat. *Journal of Hydrometeorology*, *15*(1), 117–142. https://doi.org/10.1175/JHM-D-13-026.1

Carroll, R. W. H., Bearup, L. A., Brown, W., Dong, W., Bill, M., & Willlams, K. H. (2018). Factors controlling seasonal groundwater and solute flux from snow-dominated basins. *Hydrological Processes*, *32*(14), 2187–2202. https://doi.org/10.1002/hyp.13151

Carroll, R. W. H., Deems, J. S., Niswonger, R., Schumer, R., & Williams, K. H. (2019). The importance of interflow to groundwater recharge in a snowmelt-dominated Headwater Basin. *Geophysical Research Letters*, *46*(11), 5899–5908. https://doi.org/10.1029/2019GL082447

Carroll, R. W. H., Gochis, D., & Williams, K. H. (2020). Efficiency of the summer monsoon in generating streamflow within a snow-dominated Headwater Basin of the Colorado River. *Geophysical Research Letters*, *47*(23), 1–10. https://doi.org/10.1029/2020GL090856

Claassen, H. C., & Downey, J. S. (1995). A model for deuterium and oxygen-18 isotope changes during evergreen interception of snowfall. *Water Resources Research*, *31*(3), 601–618. https://doi.org/10.1029/94WR01995

Clark, I. D., & Fritz, P. (1997). *Environmental isotopes in hydrogeology*. Lewis Publishing.

Clark, J., Meiman, J. R., & Friedman, I. (1970). Deuterium variations in an annual snowpack. *Water Resources Research*, *6*(1), 125–129. https://doi.org/10.1029/WR006i001p00125

Clark, M. P., Hendrikx, J., Slater, A. G., Kavetski, D., Anderson, B., Cullen, N. J., Kerr, T., Örn Hreinsson, E., & Woods, R. A. (2011). Representing spatial variability of snow water equivalent in hydrologic and land-surface models: A review. *Water Resources Research*, *47*(7), 1–23. https://doi.org/10.1029/2011WR010745

Clifton, A., Manes, C., Rüedi, J. D., Guala, M., & Lehning, M. (2008). On shear-driven ventilation of snow. *Boundary-Layer Meteorology*, *126*(2), 249–261. https://doi.org/10.1007/s10546-007-9235-0

Colbeck, S. C. (1989). Air movement in snow due to windpumping. *Journal of Glaciology*, *35*(120), 209–213. https://doi.org/10.3189/s0022143000004524

Cooper, L. W. (1998). Isotopic fractionation in snow cover. In *Isotope tracers in catchment hydrology* (pp. 119–136). Elsevier. https://doi.org/10.1016/b978-0-444-81546-0.50011-2

Dahlke, H. E., & Lyon, S. W. (2013). Early melt season snowpack isotopic evolution in the Tarfala valley, northern Sweden. *Annals of Glaciology*, *54*(62), 149–156. https://doi.org/10.3189/2013AoG62A232

Dansgaard, W. (1964). Stable isotopes in precipitation. *Tellus*, *16*(4), 436–468. https://doi.org/10.3402/tellusa.v16i4.8993

Earman, S., Campbell, A. R., Phillips, F. M., & Newman, B. D. (2006). Isotopic exchange between snow and atmospheric water vapor: Estimation of the snowmelt component of groundwater recharge in the southwestern United States. *Journal of Geophysical Research Atmospheres*, *111*(9), 1–18. https://doi.org/10.1029/2005JD006470

Essery, R., Li, L., & Pomeroy, J. (1999). A distributed model of blowing snow over complex terrain. *Hydrological Processes*, *13*(14–15), 2423–2438. https://doi.org/10.1002/(SICI)1099-1085(199910)13:14/15<2423::AID-HYP853>3.0.CO;2-U

Evans, S. L., Flores, A. N., Heilig, A., Kohn, M. J., Marshall, H. P., & McNamara, J. P. (2016). Isotopic evidence for lateral flow and diffusive transport, but not sublimation, in a sloped seasonal snowpack, Idaho, USA. *Geophysical Research Letters*, *43*(7), 3298–3306. https://doi.org/10.1002/2015GL067605

Fang, Z., Carroll, R. W. H., Schumer, R., Harman, C., Wilusz, D., & Williams, K. H. (2019). Streamflow partitioning and transit time distribution in snow-dominated basins as a function of climate. *Journal of Hydrology*, *570*(December 2018), 726–738. https://doi.org/10.1016/j.jhydrol.2019.01.029

Friedman, I., Benson, C., Gleason, J. I. M., & Survey, S. G. (1991). *Isotopic changes during snow metamorphism oD oD. 3*.

Friedman, I., Smith, G. I., Gleason, J. D., Warden, A., & Harriss, J. M. (1992). Stable isotope composition of waters in southeastern California 1. Modern precipitation. *Journal of Geophysical Research*, *97*, 5795–5812.

Gardner, M. A., Morton, C. G., Huntington, J. L., Niswonger, R. G., & Henson, W. R. (2018). Input data processing tools for the integrated hydrologic model GSFLOW. *Environmental Modelling and Software*, *109*(June), 41–53. https://doi.org/10.1016/j.envsoft.2018.07.020

Han, T., Zhang, M., Wang, S., Qu, D., & Du, Q. (2020). Sub-hourly variability of stable isotopes in precipitation in the marginal zone of east Asian monsoon. *Water*, *12*(8), 1–14. https://doi.org/10.3390/W12082145

Hood, E., Williams, M., & Cline, D. (1999). Sublimateion from a seasonal snowpack at a continental, mid-latidude apline site. *Hydrological Processess*, *13*, 1781–1797. https://doi.org/10.1002/(SICI)1099-1085(199909)13:12/13<1781::AID-HYP860>3.0.CO;2-C

Hürkamp, K., Zentner, N., Reckerth, A., Weishaupt, S., Wetzel, K. F., Tschiersch, J., & Stumpp, C. (2019). Spatial and temporal variability of snow isotopic composition on Mt. Zugspitze, Bavarian Alps, Germany. *Journal of Hydrology and Hydromechanics*, *67*(1), 49–58. https://doi.org/10.2478/johh-2018-0019

Immerzeel, W. W., Lutz, A. F., Andrade, M., Bahl, A., Biemans, H., Bolch, T., Hyde, S., Brumby, S., Bavies, B. J., Elmore, A. C., Emmer, A., Feng, M., Fernandez, A., Haritashya, U., Kargel, J. S., Koppes, M., Kraaijenbrink, P. D. A., Kulkarni, A. V., Mayewski, P. A., … Baillie, J. E. M. (2020). Importance and vulnerability of the world's water towers. *Nature*, *577*, 364–369. https://doi.org/10.1038/s41586-O19-1822-y

Jackson, S. I., & Prowse, T. D. (2009). Spatial variation of snowmelt and sublimation in a high-elevation semi-desert basin of western Canada. *Hydrological Processess*, *23*, 2611–2627. https://doi.org/10.1002/hyp.7320

Jasechko, S. (2019). Global isotope hydrogeology – Review. *Review of Geophysics*, *57*, 835–965. https://doi.org/10.1029/2018RG000627

Johnson, G., & Jamienson, B. (2000). Strength changes of layers of faceted snow crystals in the Columbia and Rocky Mountain snowpack climates in southwestern Canada. In *International snow science workshop*, 9. https://schulich.ucalgary.ca/asarc/files/asarc/StrChgFacets.pdf

Koeniger, P., Hubbart, J. A., Link, T., & Marshall, J. D. (2008). Isotopic variation of snow cover and streamflow in response to changes in canopy strucutre in a snow-dominated mountain catchment. *Hydrological Processes*, *22*, 557–566. https://doi.org/10.1002/hyp.6967

Kopec, B. G., Feng, X., Posmentier, E. S., & Sonder, L. J. (2019). Seasonal deuterium excess variations of precipitation at summit, Greenland, and their climatological significance. *Journal of Geophysical Research: Atmospheres*, *124*(1), 72–91. https://doi.org/10.1029/2018JD028750

Kormos, P. R. (2005). *Accountig for time and space variations of d18O in a snowmelt isotopic hydrograph seperation in the Boise front* [MS Thesis]. Boise State University.

Landfire. (2015). *Existing vegetation type and cover layers*. U.S. Department of the Interior, Geological Survey. http://landfire.cr.usgs.gov/viewer/

Lang, H. (1981). Is evaporation an important component in high alpine hydrology? *Nordic Hydrology*, *12*(4–5), 217–224. https://doi.org/10.2166/nh.1981.0017

Leavesley, G. H., Markstrom, S. L., Brewer, M. S., & Viger, R. J. (1983). The modular modeling system (MMS)—The physical process modeling component of a database-centered decision support system for water and power management. *Water, Air, and Soil Pollution*, *90*, 303–3011.

Lee, J., Feng, X., Faiia, A. M., Posmentier, E. S., Kirchner, J. W., Osterhuber, R., & Taylor, S. (2010). Isotopic evolution of a seasonal snowcover and its melt by isotopic exchange between liquid water and ice. *Chemical Geology*, *270*(1–4), 126–134. https://doi.org/10.1016/j.chemgeo.2009.11.011

MacDonald, M. K., Pomeroy, J. W., & Pietroniro, A. (2010). On the importance of sublimation to an alpine snow mass balance in the Canadian Rocky Mountains. *Hydrology and Earth System Sciences*, *14*(7), 1401–1415. https://doi.org/10.5194/hess-14-1401-2010

Marchetti, D. W., & Marchetti, S. B. (2019). Stable isotope compositions of precipitation from Gunnison, Colorado 2007–2016: Implications for the climatology of a high-elevation valley. *Heliyon*, *5*(7), e02120. https://doi.org/10.1016/j.heliyon.2019.e02120

Markstrom, S. L., Regan, R. S., Hay, L. E., Viger, R. J., Webb, R. M. T., Payn, R. A., & LaFontaine, J. H. (2015). PRMS-IV, the precipitation-runoff modeling system, version 4. *U.S. Geological Survey technical methods, Book 6*(Chapter B7), 157. https://doi.org/10.3133/tm6B7

Mott, R., Vionnet, V., & Grünewald, T. (2018). The seasonal snow cover dynamics: Review on wind-driven coupling processes. *Frontiers in Earth Science*, *6*(December), 1–25. https://doi.org/10.3389/feart.2018.00197

O'Neil, J. R. (1977). Stable isotopes in mineralogy. *Physics and Chemistry of Minerals*, *2*(1–2), 105–123. https://doi.org/10.1007/BF00307527

Otte, I., Detsch, F., Gütlein, A., Scholl, M., Kiese, R., Appelhans, T., & Nauss, T. (2017). Seasonality of stable isotope composition of

atmospheric water input at the southern slopes of Mt. Kilimanjaro, Tanzania. *Hydrological Processes*, *31*(22), 3932–3947. https://doi.org/10.1002/hyp.11311

Putman, A. L., Feng, X., Sonder, L. J., & Posmentier, E. S. (2017). Annual variation in event-scale precipitation δ2H at barrow, AK, reflects vapor source region. *Atmospheric Chemistry and Physics*, *17*(7), 4627–4639. https://doi.org/10.5194/acp-17-4627-2017

Putman, A. L., Fiorella, R. P., Bowen, G. J., & Cai, Z. (2019). Global perspective on local MeteoricWater lines: Meta-analytic insight into fundamental controls and practical constraints. *Water Resources Research*, *55*, 6896–6910. https://doi.org/10.1029/2019WR025181

Schlaepfer, D. R., Ewers, B. E., Shuman, B. N., Williams, D. G., Frank, J. M., Massman, W. J., & Lauenroth, W. K. (2014). Terrestrial water fluxes dominated by transpiration: Comment. *Ecosphere*, *5*(5), 1–9. https://doi.org/10.1890/ES13-00391.1

Sexstone, G. A., Clow, D. W., Fassnacht, S. R., Liston, G. E., Hiemstra, C. A., Knowles, J. F., & Penn, C. A. (2018). Snow sublimation in mountain environments and its sensitivity to forest disturbance and climate warming. *Water Resources Research*, *54*(2), 1191–1211. https://doi.org/10.1002/2017WR021172

Sinclair, K. E., & Marshall, S. J. (2008). Post-depositional modification of stable water isotops in winter snowpacks in the Canadian Rocky Mountains. *Annals of Glaciology*, *49*, 96–106. https://doi.org/10.3189/172756408787814979

Stichler, W., Rauert, W., & Martinec, J. (1981). Environmental isotope studies of an alpine snowpack (Weissfluhsoch Switzerland). *Nordic Hydrology*, *12*(4–5), 297–308. https://doi.org/10.2166/nh.1981.0024

Stichler, W., Schotterer, U., Fröhlich, K., Ginot, P., Kull, C., Gäggeler, H., & Pouyaud, B. (2001). Influence of sublimation on stable isotope records recovered from high-altitude glaciers in the tropical Andes. *Journal of Geophysical Research – Amospheres*, *106*(D19), 22613–22620. https://doi.org/10.1029/2001JD900179

Stigter, E. E., Litt, M., Steiner, J. F., Bonekamp, P. N. J., Shea, J. M., Bierkens, M. F. P., & Immerzeel, W. W. (2018). The importance of snow sublimation on a Himalayan glacier. *Frontiers in Earth Science*, *6*-(August), 1–16. https://doi.org/10.3389/feart.2018.00108

Svoma, B. M. (2016). Difficulties in determining snowpack sublimation in complex terrain at the macroscale. *Advances in Meteorology*, *2016*, 1–10. https://doi.org/10.1155/2016/9695757

Tappa, D. J., Kohn, M. J., McNamara, J. P., Benner, S. G., & Flores, A. N. (2016). Isotopic composition of precipitation in a topographically steep, seasonally snow-dominated watershed and implications of variations from the global meteoric water line. *Hydrological Processess*, *30*, 4582–4592. https://doi.org/10.1002/hyp.10940

Taylor, S., Feng, X., Kirchner, J. W., Osterhuber, R., Klaue, B., & Renshaw, C. E. (2001). Isotopic evolution of a seasonal snowpack and its melt. *Water Resources Research*, *37*(3), 759–769. https://doi.org/10.1029/2000WR900341

Taylor, S., Feng, X., Williams, M., & McNamara, J. (2002). How isotopic fractionation of snowmelt affects hydrograph separation. *Hydrological Processes*, *16*(18), 3683–3690. https://doi.org/10.1002/hyp.1232

Tennant, C. J., Harpold, A., Lohse, K. A., Godsey, S. E., Crosby, B. T., Larsen, L. G., Brooks, P. D., Van Kirk, R. W., & Glen, N. F. (2017). Regional sensitivities of seasonal snowpack to elevation, aspect, and vegetation cover in western North America. *Water Resources Research*, *53*, 6908–6926. https://doi.org/10.1002/2016/WR019374

U.S. Geological Survey. (2019). *National Elevation Dataset (NED)*. https://catalog.data.gov/dataset/usgs-national-elevation-dataset-ned

Unnikrishna, P. V., McDonnell, J. J., & Kendall, C. (2002). Isotope variations in a Sierra Nevada snowpack and their relation to meltwater. *Journal of Hydrology*, *260*(1–4), 38–57. https://doi.org/10.1016/S0022-1694(01)00596-0

Varadharajan, C., Faybishenko, B., Henderson, A., Henderson, M., Hendrix, V. C., Hubbard, S. S., Kakalia, Z., Newman, A., Potter, B., Steltzer, H., Versteeg, R., Agarwal, D. A., Williams, K. H., Wilmer, C., Wu, Y., Brown, W., Burrus, M., Carroll, R. W. H., Christianson, D. S., … Enquist, B. J. (2019). Challenges in building an end-to-end system for acquisition, management, and integration of diverse data from sensor networks in watersheds: Lessons from a mountainous community observatory in East River, Colorado. *IEEE Access*, *7*, 182796–182813. https://doi.org/10.1109/ACCESS.2019.2957793

Vreča, P., & Kern, Z. (2020). Use of water isotopes in hydrological processes. *Water*, *12*(8), 1–6. https://doi.org/10.3390/w12082227

Wang, Z., Huang, N., & Pähtz, T. (2019). The effect of turbulence on drifting snow sublimation. *Geophysical Research Letters*, *46*(20), 11568–11575. https://doi.org/10.1029/2019GL083636

Zhang, T., Osterkamp, T., Stamnes, K. (1996). Influence of the depth hoar layer of the seasonal snow cover on the ground thermal regime. *Water Resources Research*. *32*(7), 2075–2086. https://doi.org/10.1029/96WR00996

SUPPORTING INFORMATION

Additional supporting information can be found online in the Supporting Information section at the end of this article.

How to cite this article: Carroll, R. W. H., Deems, J., Maxwell, R., Sprenger, M., Brown, W., Newman, A., Beutler, C., Bill, M., Hubbard, S. S., & Williams, K. H. (2022). Variability in observed stable water isotopes in snowpack across a mountainous watershed in Colorado. *Hydrological Processes*, *36*(8), e14653. https://doi.org/10.1002/hyp.14653